

## 3-2-9 A Storm-Time Super Bubble as Observed with Dense GPS Receiver Network at East Asian Longitudes

MA Guanyi and MARUYAMA Takashi

A post sunset plasma bubble manifested by TEC depletion was observed at midlatitudes ( $\sim 30\text{--}34^\circ\text{ N}$ ,  $\sim 130\text{--}134^\circ\text{ E}$ ) during the main phase of a geomagnetic storm on 12 February 2000. The storm was characterized by southward turning of IMF  $B_z$  preceded with storm sudden commencement. With loss of lock and ROTI maps, the bubble was seen to bifurcate at the early growth phase of the storm. The upward drift speed was observed  $\sim 300\text{ m/s}$  at  $\sim 2150\text{ km}$ , and decreasing with increasing altitude and time. The bubble had unusually large latitudinal extension reaching midlatitude of  $36.5^\circ\text{ N}$  ( $31.5^\circ\text{ N}$  magnetic latitude), indicating an apex height of  $\sim 2550\text{ km}$  at the magnetic equator. In process of the evolution, the bubble drifted eastward at a speed of  $\sim 50\text{ m/s}$ . The  $F$  region peak height and density obtained by a meridional ionosonde chain suggested a prompt penetrating magnetospheric electric field helped to trigger the super bubble.

### Keywords

Plasma bubble, Magnetic storm, ROTI map, Loss of lock, GPS

### 1 Introduction

The term “bubble” refers to the low density plasma region in the nighttime equatorial ionosphere that contains strong irregularities. The dynamic processes and the spatial morphology of plasma bubbles have been studied by radio and optical observations, rocket measurements and numerical simulations [1]–[7]. It has been generally understood that plasma bubbles are formed in association with nonlinear Rayleigh-Taylor process at the bottomside of the  $F$  region, and rise to the topside ionosphere. Specifically during the post-sunset period, the bottomside of the equatorial  $F$  region often becomes unstable resulted from a complex interaction of electric fields, neutral winds and the earth’s magnetic field. On some evenings, a perturbation in the unstable bottomside grows nonlinearly into a bubble. The bubble will rise by the effect of buoyancy up

to where the density entrapped in the bubble is equal to that of the surroundings. Confined by the geomagnetic field, plasma bubbles extend in latitude away from the magnetic equator while rising up. In the east-west they have elongated, wedge-like structure which often drift eastward. Though basic scenario is clear, the problem remains concerning the seeding and the evolution of the plasma bubbles [8]–[10].

With L-band signals traveling through the ionosphere, the Global Positioning System (GPS) provides an excellent means to study the ionospheric irregularities. The irregularity caused scintillation can be observed by recording the fluctuations of amplitude and phase of the GPS satellite signals [11][12]. Propagation effects on GPS signals also allow measurement of the total electron content (TEC) of the ionosphere [13], and plasma bubbles can be detected as TEC depletions when they happen to orient along the path from a

GPS satellite to a GPS receiver [14]. Furthermore the rate of change of the TEC, termed ROT, and the rate of TEC index based on the standard deviation of ROT, termed ROTI, have been utilized to investigate the irregularities since these parameters characterize phase fluctuations of the GPS signals due to the effects of ionospheric irregularities [15]–[17]. As the GPS can be used for various purposes, the ground-based GPS receivers and hence networks have been increasingly set up worldwide. This enables studies of the ionosphere on a large regional or global scale. Time evolution and spatial structure of plasma bubbles can be examined in detail [16].

A dense GPS Earth Observation Network (GEONET) has been set up in Japan since 1994. It consists of more than 1200 dual frequency GPS receivers [18]. In the last few years, midlatitude ionospheric events have been studied by using observations from GEONET [19]–[21]. Recently, a statistical study of ionospheric irregularities was made with GEONET ROTI ( $> 0.1$  TECU/min), and two-dimensional ROTI maps were shown on the night of 12 February 2000 when a geomagnetic storm was preceded [22]. Here a different aspect of the same event is presented with the same GPS network. A stormtime equatorial bubble is found by the GEONET TEC and confirmed by the ion density measurements by the Defense Meteorological Satellite Program (DMSP) F14 satellite. A striking feature of this bubble is its mid-latitude extension. This is the first case the evolution of a bubble is examined by using GEONET ROTI. The ROTI map made from GEONET enabled study of the irregularities on much larger scale than any other observation means.

## 2 Observations

Each receiver of the GEONET provides the carrier phase and pseudorange of the dual frequency GPS signals at 30-s intervals. The ionospheric TEC from a GPS satellite to a GPS receiver can be obtained from the differences

between pseudoranges or phases of the two signals. Using around 300 GPS receivers selected homogeneously from GEONET, the TEC over Japan is calculated with a temporal resolution of 15-min and a spatial resolution of  $2^\circ \times 2^\circ$  in longitude and latitude [23]. ROTI maps were made from phase measurements by the same receivers used for TEC calculation and by projecting the ROTI values on the Earth from the ionospheric pierce point at 400 km altitude. A relative slant TEC was first obtained from the differential phase at 30-s intervals. Then ROT was determined by taking the difference between the slant TECs at two successive times. The ROTI is defined as the standard deviation of ROT, given by  $\sqrt{\langle \text{ROT}^2 \rangle - \langle \text{ROT} \rangle^2}$  for each 5-min interval [16]. When calculating TEC and ROTI, only data from those satellites whose elevation angle was larger than  $30^\circ$  were used, to reduce multi-path effects.

When the irregularity has strong density variation, a GPS receiver could not track the fluctuation of the GPS signal passing through. This is often referred to as loss of lock. Here, loss of lock is used to represent the existence of the irregularities.

DMSP are sun-synchronous polar orbiting satellites. They were launched to investigate the Earth's environment from an altitude of  $\sim 840$  km to  $\sim 880$  km. The ion density they measured provides a direct means to identify plasma bubbles.

Another set of data is from a chain of ionosonde observations at Okinawa ( $26.3^\circ$  N,  $127.8^\circ$  E;  $20.7^\circ$  N magnetic latitude), Kokubunji ( $35.7^\circ$  N,  $139.5^\circ$  E;  $30.0^\circ$  N magnetic latitude) and Wakkanai ( $45.4^\circ$  N,  $141.7^\circ$  E;  $40.5^\circ$  N magnetic latitude) in Japan. The ionospheric critical frequencies,  $f_oF_2$ , and the maximum usable frequency for a 3000 km range,  $M(3000)F_2$ , were mainly scaled from the ionograms. Then the maximum electron density,  $N_mF_2$ , can be obtained by  $N_mF_2 = 1.24 \times 10^{10} f_oF_2$ . And the height of the  $F$  peak was estimated from an empirical formula  $h_mF_2 = -176 + 1490 / M(3000)F_2$  [24].

Data used to describe the geomagnetic conditions are, the interplanetary magnetic

field (IMF)  $B_z$  component observed by the Advanced Composition Explorer (ACE) spacecraft, the longitudinal asymmetric index  $ASY-H$  and the symmetric index  $SYM-H$  of the ring current, and the geomagnetic index  $K_p$ . The  $ASY-H$  is a good indicator of the auroral substorm activity, and the  $SYM-H$  is essentially the same as the  $D_{st}$  index.

## 2.1 Geomagnetic storm

An SSC, associated with IMF  $B_z$  changes, signaled the onset of a magnetic storm at 2353 UT on 11 February 2000, as indicated by its signatures in the  $ASY-H/SYM-H$  and  $K_p$  indices in Fig. 1. About 8 hours later at 0800 UT on 12 February, the IMF  $B_z$  turned southward abruptly. The magnetic field started to decrease monotonously, with rate of change of,  $-95$  nT/hr for 0835–0904 UT, and  $-144$  nT/hr for 0953–1008 UT. It reached its maximum depression of  $-165$  nT in 4 hours at 1200 UT,

when the IMF  $B_z$  turned northward. Though the IMF  $B_z$  turned southward again a few minutes later, the storm was not enhanced as shown by the geomagnetic indices.

## 2.2 Stormtime plasma bubble

Equatorial plasma bubbles can be detected as TEC depletions. Figure 2 gives the TEC at low and mid-latitudes for the day of 12 February 2000 (dots connected with line). The solid lines are taken as a reference, which represent the average TEC for the previous quiet days. Corresponding to the storm, an enhancement of TEC was observed around 0800 UT and lasted for about 16 hours on 12 February. It is noticeable that the TEC increased further and maintained its higher level from 1030 to 1500 UT. Within this period an apparent TEC depletion appeared at ( $31^\circ$  N,  $131^\circ$  E) and its nearby area, as indicated by dashed vertical lines from 1115 to 1315 UT in Fig. 2. The

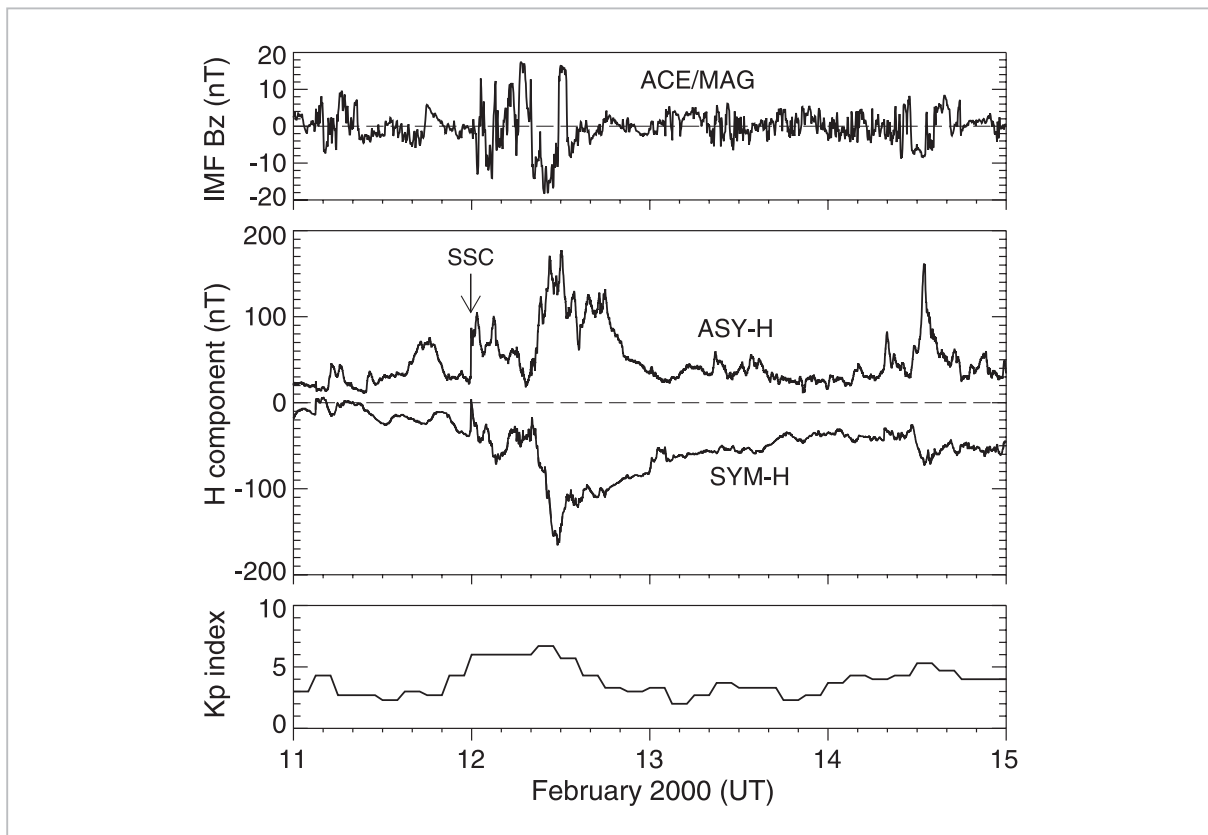


**Fig. 1** IMF  $B_z$  and geomagnetic indices from 11–15 February 2000

The IMF  $B_z$  was plotted with a time delay of 50 min to account for the propagation of the solar wind from L1 point to the magnetosphere at the measured speed of  $\sim 500$  km/s.

depletion can be as large as 30 TECU less than the background. Meanwhile, DMSP F14 happened to overfly the TEC depletion region. As shown in the bottom panel of Fig. 2, it recorded ion density ( $N_i$ ) depletions at 860 km between the magnetic equator ( $8^\circ$  N,  $141^\circ$  E) and a low latitude at the Western Pacific Ocean ( $29^\circ$  N,  $136^\circ$  E) from 1114 to 1121 UT (thick line). This indicates that the TEC depletion was associated with an equatorial bubble. Taken as a reference,  $N_i$  on the previous day

when F14 made a close transit is also shown (thin line). The stormtime  $N_i$  was larger than the quiet one, which is consistent with the TEC observation. And equatorial anomaly developed compared with the previous day.

Data outages resulted from loss of lock were found to a few satellites for those receivers within or near the TEC depletion region. Because there were more than three GPS satellites with the sight of a GPS receiver, and the related signals propagate through

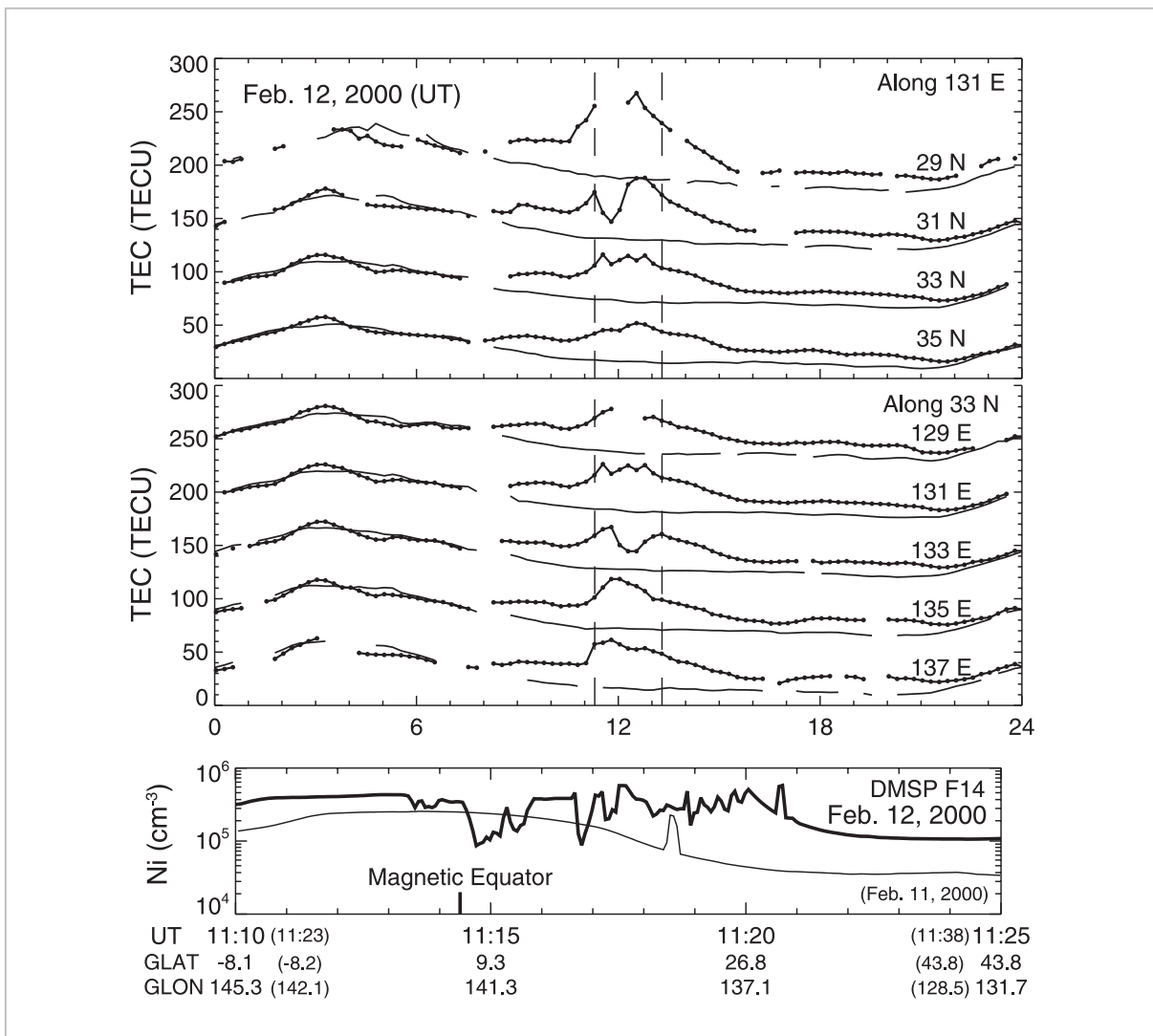


**Fig.2** Time variation of total electron content (upper panel) and latitudinal variation of total ion density as observed by the DMSP satellite (lower panel)

Thick lines with dots are TEC derived from GEONET for the storm day of 12 February 2000. Thin lines represent reference TEC, which are averaged from 9–11 February 2000. The dashed vertical lines show the period of TEC depletion. Shown in the bottom panel is the DMSP F14 observation of ion density in the nightside equatorial ionosphere. GLAT and GLON refer to geographic latitude and longitude. Shown in parentheses are time and position parameters for F14 on the previous day.

different path, it did not affect the TEC derivation for those areas where dense receivers locate, which was often the case in this study.

### 2.3 Evolution of the bubble

For the period when the TEC depletion was observed, ROTI maps are plotted as a function of latitude and longitude from about 300 GEONET-based GPS receivers' phase measurements at intervals of 5 min. Figure 3 shows the ROTI maps at 9 different times that can represent the process of the irregularities' evolution and decadence from 1105 to

1340 UT. The color bar in the figure defines 5 levels of ROTI, with white for  $0 \leq \text{ROTI} < 0.5$ ; light blue for  $0.5 \leq \text{ROTI} < 1$ ; dark blue for  $1 \leq \text{ROTI} < 1.5$ ; black for  $1.5 \leq \text{ROTI} < 2$ , and yellow for  $\text{ROTI} \geq 2$ . The red color represents loss of channel lock for a receiver-satellite pair. It can be that loss of lock occurred to both L1 and L2 signals. Here, most of the cases were loss of L2 signal lock while only pseudorange was measured for L1, which is consistent with the previous study [25].

The irregularities were first seen on the east of Okinawa between ( $23^\circ \text{ N}$ ,  $131^\circ \text{ E}$ ) and

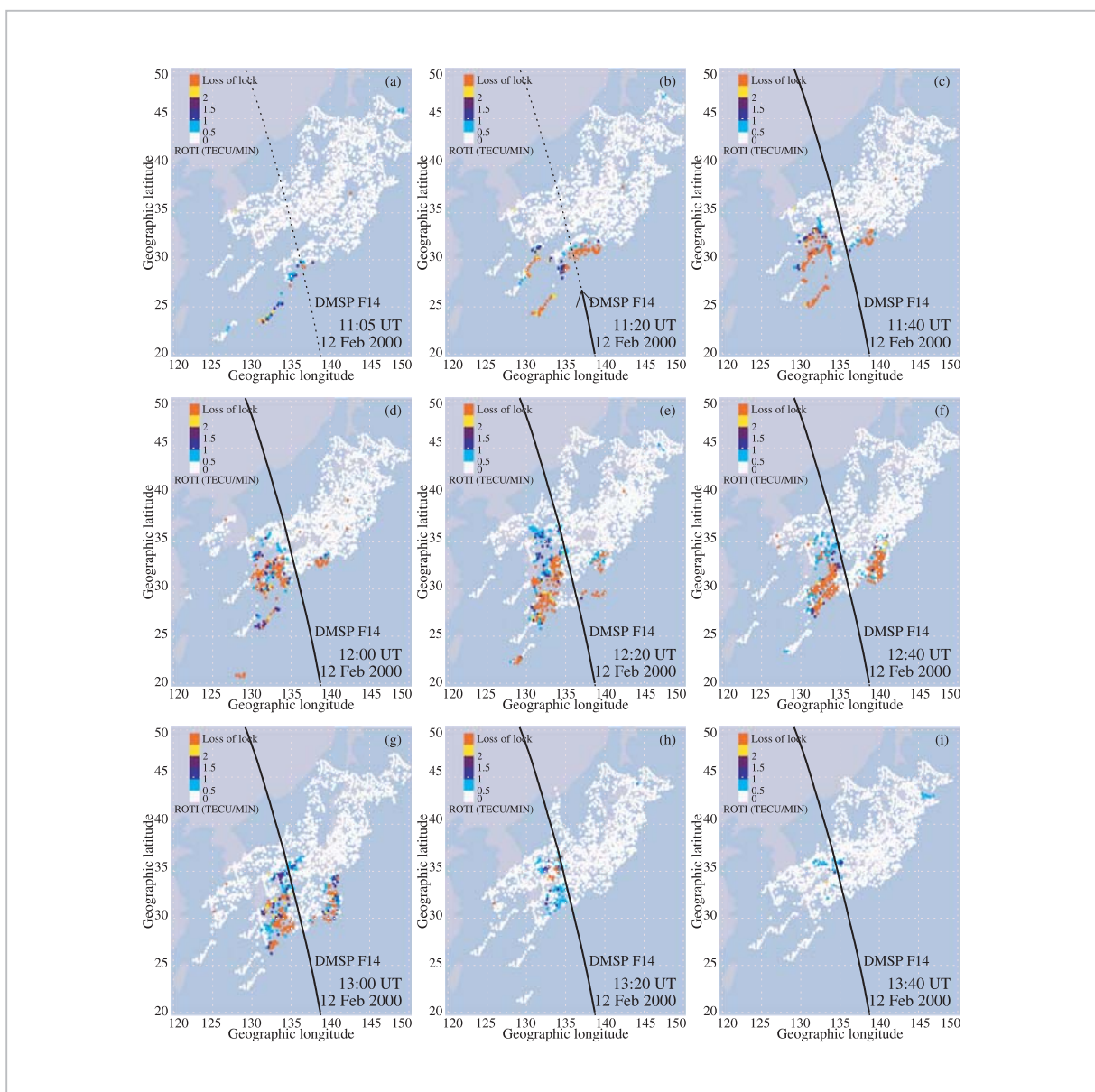


**Fig.3** Loss of lock and ROTI maps showing the temporal and spatial evolution of the plasma bubble

(30° N, 136° E) by the GEONET around 1105 UT (Fig. 3a). The local times at these longitudes were between 1949–2009 LT. The bubble from then on expanded northward as shown in Fig. 3b. The black line shows the trace of DMSP F14, and the arrow marks its position (27° N, 137° E) at 1120 UT. The highest latitude of the irregularities was ~32° N, the apex height (equatorial crossing altitude, as the following Fig. 4 shows) at this time was 1800 km. As shown in Fig. 3c, it began to exhibit two separated portions at 1140 UT, which could be bifurcated branches as often reported previously. The west side of the bubble came to latitude of 34.5° N, and the east side reached 33° N. At this time the apex height is 2150 km, and the upward drift speed of the bubble mapped onto the magnetic equator was estimated to be 300 m/s from the consecutive two ROTI maps. At 1200 UT shown in Fig. 3d, the west and east sides of the bubble came to latitudes of 36° N and 33.5° N. And the apex height is 2420 km. The upward

drift speed is estimated to be 230 m/s. In Fig. 3e the bubble moved further north and the west and east sides of the bubble reached latitudes of 36.5° N and 34° N at 1220 UT, respectively. The west side rose to an apex height of 2550 km. The upward drift slowed down to ~100 m/s. Small eastward drift as 50 m/s can be estimated by comparing the disturbance area at different times.

By 1240 UT (Fig. 3f), the northward expansion of the bubble stopped for the west side structure, while the east side reached 35.5° N near where Kokubunji ionosonde is located. Moreover, the bubble's zonal dimension seemed to shrink. Then the decline of the bubble continued. ROTI map at 1300 UT in Fig. 3g shows the bubble continued drifting eastward while shrinking. At 1320 UT, only the west side structure remained in the map. It is notable that loss of lock area decreased greatly (Fig. 3h). The east side structure disappeared around 1310 UT (not shown). Because the data is not available to the east of Japan, it is hard to tell the structure decayed or drift further eastward. No more loss of lock existed at 1340 UT (Fig. 3i). The west side structure shrunk to (35° N, 134° E) with ROTI values around 0.5~1.5. Residue of the west side structure with several light blue dots ( $0.5 \leq \text{ROTI} < 1$ ) continued drifting eastward at a speed of ~50 m/s until 1430 UT (not shown). It should be pointed out that the duration of the bubble's active state (having loss of lock), 1120–1320 UT, corresponded to the duration of the TEC depletion.

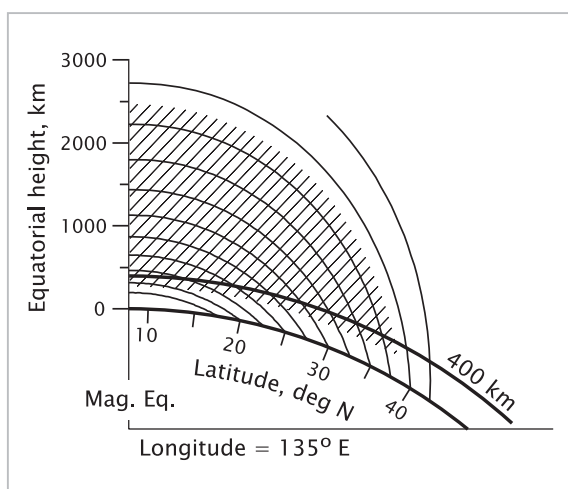


**Fig.4** A sketch of the plasma bubble and the Earth's magnetic field lines at a meridian plane over Japan

The apex height of the bubble can be estimated by mapping the ionospheric piercing point (IPP) along the magnetic field line to the equator. Here, the IPP is the intersection of the GPS signal ray path and the thin shell ionosphere, which is shown with a line at 400 km above the Earth. The geomagnetic field is determined from the International Geomagnetic Reference Field (IGRF).

## 2.4 Evidence for an eastward electric field

Figure 5 shows the ionospheric height ( $h_m F_2$ ) variation at three ionosonde stations (upper panel) on 12 February. The maximum electron density of the ionospheric  $F$  region ( $N_m F_2$ ) and the TEC at the three stations were also shown together, in the middle and lower panel. As indicated by the dot-dash lines, upward excursion in  $h_m F_2$  at the three stations started at around 1900 JST (1000 UT) and ceased one hour later at 2000 JST (1100 UT).

The magnitude of the height increase was ~90 km at Okinawa, ~40 km at Kokubunji and ~10 km at Wakkanai. At a slightly later time after the uplifting of the  $F$  region, the  $N_mF_2$  at

Okinawa increased greatly, as shown in the middle panel. The enhancement at Kokubunji was too small to be recognized. No change can be observed at Wakkanai. Similar results

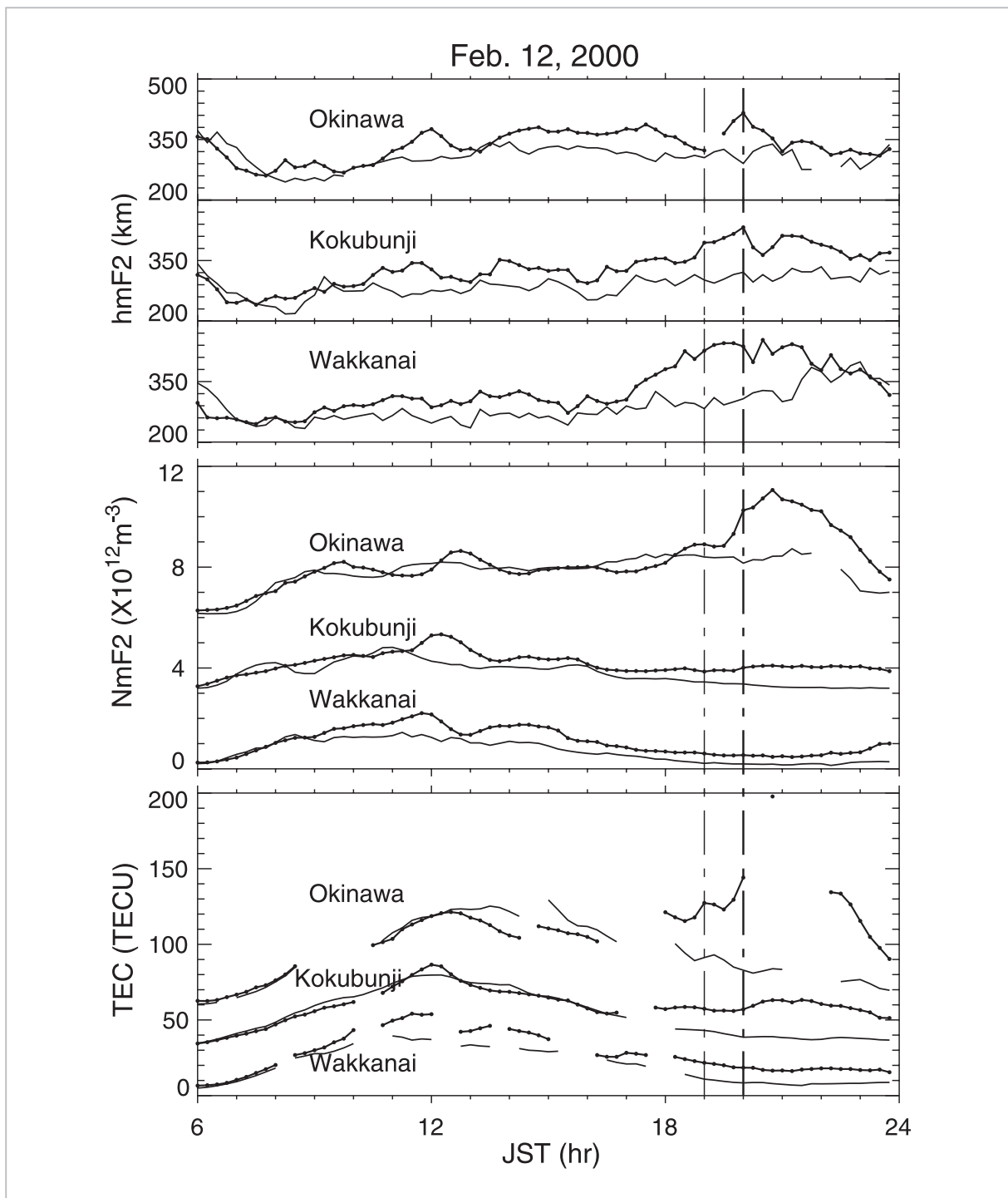


**Fig.5** Ionospheric peak height and density variations at three ionosonde stations in a meridional chain at the upper two panels

TEC over the stations are also shown at the bottom panel. Dots connected lines are for the storm day of 12 February 2000. Taken as a reference, thin lines are the same parameters on quiet day of 5 February 2000. The dot dashed vertical lines show the period of the  $F$  region uplifting.

can be found in TEC in the lower panel, but the TEC at Kokubunji apparently increased.

The uplifting of the  $F$  region and the density or TEC increase can be explained in terms of prompt penetration of an eastward electric field during the storm main phase. These ionospheric disturbances suggested that the eastward electric field imposed on the equatorial ionosphere caused the ionization anomaly to expand toward the midlatitude. From the fact that the prompt penetration occurred after sunset, it can be inferred that the TEC increase was limited in the equatorial anomaly region and a positive storm would not be formed at the high latitude [26]. The plasma bubble was observed soon after the enhancement of the eastward electric field.

It is noted that after the appearance of TEC depletion spread  $F$  was observed for the period of 1215–1715 UT at Kokubunji and 1130–2130 UT at Wakkanai [20]. No spread  $F$  was observed at Okinawa as expected. The spread  $F$  related irregularities at Wakkanai were not due to the equatorial bubble, and the generation of those at Kokubunji needs detailed assessment that is out of this paper's scope.

### 3 Discussion

Equatorial plasma bubbles develop in the bottom side of the  $F$  region where the generalized Rayleigh-Taylor instability driven by the gravitational force and eastward electric field operates. During magnetic disturbances, the eastward electric field imposed over low latitudes can arise from (1) prompt penetration of magnetospheric electric field; (2) electric field due to ionospheric disturbance dynamo [27]. The prompt penetrating electric fields can have significant amplitudes but only for periods of about one hour, and the electric fields generated by the dynamo action of stormtime disturbance wind are proportional to the energy input into the high latitude ionosphere and have longer lifetimes [28]. The rapid change of  $D_{st}$  often signifies the prompt penetration of high latitude electric fields [29][30]. Returning

to Fig. 1, a rate of change of  $SYM-H$  reached  $-144$  nT/hr for 0953–1008 UT, having a good time correlation with the simultaneous uplift of the  $F$  region at the three stations shown in the upper panel of Fig. 5. It can be concluded that the postsunset ionospheric disturbances observed at the three ionosonde stations were caused by a prompt penetration of magnetospheric eastward electric field.

It should be noted that equatorial bubbles are not often observed at midlatitudes, bubble-like plasma depletions were reported though [10][31]. The magnetic storm induced bubble discussed in this paper reached a latitude of  $\sim 36.5^\circ$  N ( $31.5^\circ$  N magnetic latitude), indicating an apex height of  $\sim 2500$  km. During the growth phase, seen from an apex height of 1800 km, the upward drift speed varied from  $\sim 300$ ,  $\sim 200$  to  $\sim 100$  m/s at the time 1140, 1200, and 1220 UT, decreasing with increasing altitude and time. The speeds were consistent with previous radar and satellite observations, but the apex height was much larger than previous records [32][33]. It is reasonable to name it as a super plasma bubble.

Generally, the bubble drift shows an eastward acceleration during its growth phase to approach the speed of the ambient plasma and of the background neutral wind which typically peaks around 150 m/s and 2100 LT [9][34]. The super bubble drifted slightly eastward, with a speed  $\sim 50$  m/s much smaller than that under normal conditions. A possible explanation can attribute to westward wind arising from Coriolis action on an equatorward wind which was produced by auroral heating during magnetic storms. The thermospheric circulation disturbances generate a poleward electric field [27]. This northward electric field is superimposed upon the background quiet-day drift pattern, which lowered the eastward bubble drift velocity. Actually in the upper panel of Fig. 5, the  $F$  region can be seen higher than the reference during the day, indicating an enhanced equatorward wind. Recently a magnetospheric disturbance induced bubble was observed in Brazilian sector to drift westward until early morning hours, and Hall electric

field was discussed as a possible cause [9]. Furthermore, several processes are mostly likely act together to cause the bubble to drift eastward slowly. Model work and more case studies are needed to clarify the dynamics of stormtime super plasma bubbles.

## 4 Conclusion

A stormtime premidnight super bubble development with bifurcated structure was detected with GPS loss of lock and ROTI maps derived from the observation by the GEONET. *F* region peak parameters obtained by a meridional ionosonde chain showed that the bubble was initiated by a prompt penetration of magnetospheric eastward electric field to equatorial latitude. The upward drift speed mapped onto the magnetic equator was estimated as  $\sim 300$  m/s at  $\sim 2150$  km, and decreasing with increasing altitude and time. The highest latitude the bubble reached was

$\sim 36.5^\circ$  N ( $31.5^\circ$  N magnetic latitude), indicating an apex height of  $\sim 2550$  km. In the whole evolution process the bubble drifted eastward at a speed of  $\sim 50$  m/s. It is shown in the paper that the densest GPS network GEONET in the world provides a unique means to study low- to midlatitudes extended bubbles or midlatitude borne irregularities in a high resolution of time and space.

## Acknowledgments

Part of this work was carried out when one of the authors (GM) held a visiting scholarship in National Institute of Information and Communications Technology of Japan. Thanks are due to Maho Nakamura for scaling the ionograms. We gratefully acknowledge the Center for Space Sciences at the University of Texas at Dallas and the US Air Force for providing the DMSP thermal plasma data.

## References

- 1 R. F. Woodman and C. La Hoz, "Radar observations of *F* region equatorial irregularities," *J. Geophys. Res.*, Vol. 81, pp. 5447–5466, 1976.
- 2 J. P. McClure, W. B. Hanson, and J. F. Hoffman, "Plasma bubbles and irregularities in the equatorial ionosphere," *J. Geophys. Res.*, Vol. 82, pp. 2650–2656, 1977.
- 3 R. T. Tsunoda, "Magnetic-field-aligned characteristics of plasma bubbles in the nighttime equatorial ionosphere," *J. Atmos. Terr. Phys.*, Vol. 42, pp. 743–752, 1980.
- 4 R. T. Tsunoda, R. T. Livingston, J. P. McClure, and W. B. Hanson, "Equatorial plasma bubbles: Vertical elongated wedges from the bottomside *F* layer," *J. Geophys. Res.*, Vol. 87, pp. 9171–9180, 1982.
- 5 K. Shiokawa, Y. Otsuka, T. Ogawa, and P. Wilkinson, "Time evolution of high-altitude plasma bubbles imaged at geomagnetic conjugate points," *Ann. Geophys.*, Vol. 22, pp. 3137–3143, 2004.
- 6 S. L. Ossakow, "Spread-*F* theories," *J. Atmos. Terr. Phys.*, Vol. 43, pp. 437–452, 1981.
- 7 S. T. Zalesak, S. L. Ossakow, and P. K. Chaturvedi, "Nonlinear equatorial spread *F* – the effect of neutral winds and background Pedersen conductivity," *J. Geophys. Res.*, Vol. 87, pp. 151–166, 1982.
- 8 R. F. Woodman, "Spread *F* – an old equatorial aeronomy problem finally resolved," *Ann. Geophys.*, Vol. 27, pp. 1915–1934, 2009.
- 9 M. A. Abdu, I. S. Batista, H. Takahashi, J. MacDougall, J. H. Sobral, A. F. Medeiros, and N. B. Trivedi, "Magnetospheric disturbance induced equatorial plasma bubble development and dynamics: A case study in Brazilian sector," *J. Geophys. Res.*, Vol. 108, 1449, doi:10.1029/2002JA009721, 2003.
- 10 C.-S. Huang, J. C. Foster, and Y. Sahai, "Significant depletions of the ionospheric plasma density at middle latitudes: A possible signature of equatorial spread *F* bubbles near the plasmopause," *J. Geophys. Res.*, Vol. 112, A05315, doi:10.1029/2007JA012307, 2007.

- 11 A. J. Van Dierendonck, J. Klobuchar, and Q. Hua, "Ionosphere scintillation monitoring using commercial single frequency C/A code receivers," Proceedings of ION GPS-93, Salt Lake City, UT, September 1993, pp. 1333–1342, 1993.
- 12 B. M. Ledvina, J. J. Makela, and P. M. Kintner, "First observations of intense GPS L1 amplitude scintillations at midlatitude," *Geophys. Res. Lett.*, Vol. 29, No. 14, 1659, doi:10.1029/2002GL014770, 2002.
- 13 G. E. Lanyi and T. Roth, "A comparison of mapped and measured total ionospheric electron content using Global Positioning System and beacon satellites observations," *Radio Sci.*, Vol. 23, pp. 483–492, 1988.
- 14 C. E. Valladares, J. Villalobos, R. Sheehan, and M. P. Hagan, "Latitudinal extension of low-latitude scintillations measured with a network of GPS receivers," *Ann. Geophys.*, Vol. 22, pp. 3155–3175, 2004.
- 15 J. Aarons, M. Mendillo, R. Yantosca, and E. Kudeki, "GPS phase fluctuations in the equatorial region during the MISETA 1994 campaign," *J. Geophys. Res.*, Vol. 101, pp. 26851–26862, 1996.
- 16 X. Pi, A. J. Mannucci, U. J. Lindqwister, and C. M. Ho, "Monitoring of global ionospheric irregularities using the worldwide GPS network," *Geophys. Res. Lett.*, Vol. 24, pp. 2283–2486, 1997.
- 17 S. Basu, K. M. Groves, J. M. Quinn, and P. Doherty, "A comparison of TEC fluctuations and scintillations at Ascension Island," *J. Atmos. Solar-Terr. Phys.*, Vol. 61, pp. 1219–1226, 1999.
- 18 S. Miyazaki, T. Saito, M. Sasaki, Y. Hatanaka, and Y. Iimura, "Expansion of GSI's nationwide GPS array," *Bull. Geogr. Surv. Inst.*, Vol. 43, pp. 23–34, 1997.
- 19 A. Saito, S. Fukao, and S. Miyazaki, "High resolution mapping of TEC perturbations with the GSI GPS network over Japan," *Geophys. Res. Lett.*, Vol. 25, pp. 3079–3082, 1998.
- 20 Y. Sahai, K. Shiokawa, Y. Otsuka, C. Ihara, T. Ogawa, K. Igarashi, S. Miyazaki, and A. Saito, "Imaging observations of midlatitude ionospheric disturbances during the geomagnetic storm of February 12, 2000," *J. Geophys. Res.*, Vol. 106, pp. 24481–24492, 2001.
- 21 T. Maruyama, G. Ma, and M. Nakamura, "Signature of TEC storm on 6 November 2001 derived from dense GPS receiver network and ionosonde chain over Japan," *J. Geophys. Res.*, Vol. 109, A10302, doi:10.1029/2004JA010451, 2004.
- 22 Y. Otsuka, T. Aramaki, T. Ogawa, and A. Saito, "A statistical study of ionospheric irregularities observed with a GPS network in Japan," *Corotating Solar Wind Streams and Recurrent Geomagnetic Activity*, *Geophys. Monogr.*, AGU, Washington, D. C., 2006.
- 23 G. Ma and T. Maruyama, "Derivation of TEC and estimation of instrumental biases from GEONET in Japan," *Ann. Geophys.*, Vol. 21, pp. 2083–2093, 2003.
- 24 T. Shimazaki, "World-wide daily variations in the height of the maximum electron density of the ionospheric  $F_2$ -layer," *J. Radio Res. Lab.*, Vol. 2, pp. 85–97, 1955.
- 25 S. Datta-Barua, P. H. Doherty, S. H. Delay, "Ionospheric scintillation effects on single and dual frequency GPS positioning," *ION GPS/GNSS 2003*, Portland, Oregon, 2003.
- 26 T. Maruyama, G. Ma, and M. Nakamura, "Observations of TEC disturbances with GEONET – TEC storm and SED –," *Special Issue of This NICT Journal*, 3-3-1, 2009.
- 27 M. Blanc and A. D. Richmond, "The ionospheric disturbance dynamo," *J. Geophys. Res.*, Vol. 85, pp. 1669–1686, 1980.
- 28 B. G. Fejer and L. Scherliess, "Time dependent response of equatorial ionospheric electric fields to magnetospheric disturbances," *Geophys. Res. Lett.*, Vol. 22, pp. 851–854, 1995.
- 29 S. Basu, Su. Basu, K. M. Groves, E. MacKenzie, M. J. Keskinen, and F. J. Rich, "Near-simultaneous plasma structuring in the midlatitude and equatorial ionosphere during magnetic superstorms," *Geophys. Res. Lett.*, Vol. 32, L12S05, doi:10.1029/2004GL021678, 2005.

- 
- 30 C. Y. Huang, W. J. Burke, J. S. Machuzak, L. C. Gentile, and P. J. Sultan, "DMSP observations of equatorial plasma bubbles in the topside ionosphere near solar maximum," *J. Geophys. Res.*, Vol. 106, pp. 8131–8142, 2001.
- 31 J. C. Foster and F. J. Rich, "Prompt midlatitude electric field effects during severe geomagnetic storms," *J. Geophys. Res.*, Vol. 103, pp. 26367–26372, 1998.
- 32 R. T. Tsunoda, "Time evolution and dynamics of equatorial backscatter plumes: 1. Growth phase," *J. Geophys. Res.*, Vol. 86, pp. 139–149, 1981.
- 33 R. S. Dabas and B. M. Reddy, "Equatorial plasma bubble rise velocities in the Indian sector determined from multistation scintillation observations," *Radio Sci.*, Vol. 25, pp. 125–132, 1990.
- 34 C. S. Lin, T. J. Immel, H. Yeh, S. B. Mende, and J. L. Burch, "Simultaneous observations of equatorial plasma depletion by IMAGE and ROCSAT-1 satellites," *J. Geophys. Res.*, Vol. 110, A06304, doi:10.1029/2004JA010774, 2005.

---

**MA Guanyi, Ph.D.**

*Professor, National Astronomical  
Observatories, Chinese Academy of  
Sciences.*

*Upper Atmospheric Physics, Satellite  
Communication and Navigation*

**MARUYAMA Takashi, Ph.D. (Eng.)**

*Executive Researcher  
Upper Atmospheric Physics*